NATIONAL RADIO ASTRONOMY OBSERVATORY
GREEN BANK, WEST VIRGINIA

ELECTRONICS DIVISION INTERNAL REPORT NO. 190

AN 11.5 TO 15.5 GHz CORRUGATED HORN FOR THE 140-FOOT CASSEGRAIN SYSTEM

J. RICHARD FISHER

SEPTEMBER 1978

NUMBER OF COPIES: 150

AN 11.5 TO 15.5 GHz CORRUGATED HORN FOR THE 140-FOOT CASSEGRAIN SYSTEM

J. Richard Fisher

TABLE OF CONTENTS

AN 11.5 TO 15.5 GHz CORRUGATED HORN FOR THE 140-FOOT CASSEGRAIN SYSTEM

J. Richard Fisher

Summary

A single mode, corrugated, conical horn has been built for use with the X-band upconverter/maser receiver on the 140-foot telescope. This horn has a return loss of greater than 20 dB and well matched E and H plane patterns with nearly constant beamwidths between 11.5 and 15.5 GHz. The design procedure and tests are described in this report, and predictions are made for the aperture efficiency and spillover temperature when the horn is installed on the 140-foot. A bit of rationale behind the use of corrugated horns is given in the introduction, and enough detail is included in the succeeding sections to show how feeds for other frequency ranges in the Cassegrain system will be designed.

Introduction

The evolution of corrugated horns has been driven by efforts to correct some of the undesirable properties of smooth-wall horns when used as feeds for reflector antennas. Namely, corrugated horns have more nearly matched E and H plane radiation patterns, lower cross polarization, and better sidelobe suppression than smooth-wall horns. The main disadvantage of corrugated horns is that they are more difficult to construct.

The technical literature is filled with analyses of corrugated horns. An excellent collection of many of the most important papers on corrugated horns published before 1974 appears in A. W. Love's book on horn antennas [1], and a concise outline of corrugated horn design is given by Thomas [11]. A few other papers which are particularly helpful in design are by Jenken [2], Buckmeyer [3], Loefer, et al. [4], and Dragone [5], [6].

Most of the poor performance of smooth-wall horns comes from the fact that the electric field taper across the aperture is not the same in the E and H planes. In a square horn, for instance, the electric field is uniform in the E plane but has a cosine taper in the H plane. The E plane dimension can be made smaller to equalize the beamwidths in the two directions, but this only works for one sense of polarization, and it does not reduce the sidelobes associated with uniform field distribution.

Corrugated horns are not subject to this problem because the boundary conditions presented by their slotted walls to waves propagating in electromagnetic horns are the same for the E and H fields. Normally the grooves in a corrugated horn are a bit over a quarter of a wavelength deep and run transverse to the horn axis. This permits circumferential but not longitudinal currents to flow on the walls so just above the tops of the grooves longitudinal E and H fields can exist, but circumferential fields are zero. It can be said that the longitudinal surface impedance is infinite and the circumferential impedance is zero. For a wave travelling in the longitudinal direction the electric field component perpendicular to the surface must also be zero at the surface since the circumferential H field is zero. Hence, the electric field at the aperture of a corrugated horn must be tapered in both the E and H planes. The exact field distribution will depend on which of the possible modes at the aperture have been excited.

Another way of looking at the aperture field distribution is to say that at least one TE and one TM wave have combined to cancel all transverse electric fields at the aperture walls. This is a useful concept when looking at what happens at the throat of the horn where some of the power propagating in the dominant mode of the exciting waveguide must be converted into one or more other modes. The right combination of modes in a smooth-wall horn can be

generated to cancel fields at the walls (cf. Potter [7]), but in a smooth-wall guide the TE and TM modes travel at different velocities and will arrive at the aperture in the proper phase for only a narrow range of frequencies. In a corrugated guide the appropriate TE and TM modes making up a hybrid (HE) mode travel with the same phase velocity. Generating the proper proportion and phase of two modes in a smooth-wall guide is quite tricky, but in a corrugated guide the proper combination must exist. After all, the hybrid mode concept is just a "smooth wall" way of looking at a natural corrugated guide mode.

The bandwidth of a corrugated horn is limited by several factors. Ideally the corrugation slots should be $\lambda/4$ deep to satisfy the boundary conditions mentioned above. However, this depth can be as much as 0.4 λ in a narrow flare angle horn. Slots much shallower than $\lambda/4$ are not permissible because transverse surface currents are possible at the tops of such slots.

The impedance match between the exciting waveguide (usually smooth wall) and the corrugated horn also tends to limit the lowest frequency at which the horn can operate. When this waveguide gets within about 30% of its dominant mode cutoff frequency the generation of the second partner of the hybrid mode is difficult without a large impedance mismatch. A smooth flare and deeper first slots help this transition in a narrow flare angle horn.

Another criterion which determines the useful frequency range of a horn is the variation of its beamwidth with frequency. The next section will show that as long as the size of a single mode corrugated horn is not constrained this will not be as important as the factors mentioned above.

Design Principles

To illustrate the procedure used in designing the feed in this report let us talk specifically about a narrow flare angle conical horn supporting only the HE_{11} mode with the following specifications:

Frequency range	11.5 to 15.5 MHz
Maximum return loss	20 dB
Subreflector edge illumination (7°.14 half angle)	-11 dB ± 1 dB
Pattern circularity	1 dB peak to peak
Phase deviation from best-fit sphere in far field between 7°.14 half angles	± 5°

The exact frequency range was set in retrospect because I did not know how quickly the return loss would decrease at the low frequency end nor did I know at what frequency the first unwanted higher order mode would appear. Let us assume that I knew at the start what has been learned empirically to show how the next feed will be designed.

A square corrugated horn would have been easier to construct, but its cross polarization and pattern properties are poorer than those of a conical horn. An extensive comparison between square and conical corrugated horns is available in a paper by Caldecott, et al. [8].

Radiation pattern

The radiation pattern of a single mode horn is fixed by its aperture size and its length. The aperture size defines the radiating area, and the horn length determines the phase distribution of the aperture field. These two properties compete to determine the far field radiation pattern.

For a given horn size, as the operating frequency is increased the far field pattern will tend to get narrower because of the increase in the number of wavelengths across the aperture and will tend to get broader because of the increased phase variation across the aperture. These two effects can be made to balance one another to produce a nearly constant beamwidth over a frequency

range of more than 50%. The phase distribution is computed by assuming that the wavefront is a spherical surface with its origin at the feed apex.

The horn dimensions may be determined iteratively. Start with an aperture which is about twice as big as would be needed to produce the desired beamwidth with no phase error. Then calculate a feed length which will give the proper phase distribution from the following approximation for narrow flare horns:

$$L \simeq \frac{a^2}{1.4\,\lambda} \qquad (0.70\ \lambda \text{ center to edge phase variation}) \qquad (1)$$

where a is the aperture radius. Compute the far field pattern at several frequencies in the operating band to see how well the desired specifications are satisfied by the first guess and adjust the feed dimensions accordingly. The last section of this report describes the radiation pattern computation and a 9825A calculator program for this purpose.

Slot sizes

The only critical dimension of the corrugation slots in their depth. The slots should be no less than $\lambda/4$ deep at the lowest operating frequency, but near the small end of the horn slightly shallower slots are still effective at suppressing surface waves (cf. Thomas [11]). The best practice is to design the slot depths to be $\lambda/4$ at the low end of the band with the exception of a few slots which will be discussed later near the throat of the horn.

The slot density and the width of the vanes between slots affect the efficiency of surface wave attenuation, but only weakly. With a narrow flare horn there are many slots so the rapidity with which the surface wave is attenuated is not crucial. More slots per unit length and thinner vanes give better suppression. Four slots per wavelength at the high end of the frequency

range is quite adequate, and for ease in machining the vane and slot widths were chosen to be equal in the horn described here. An extensive study of the effects of various slot parameters on the performance of corrugated horn surfaces can be found in a paper by Terzuoli, et al. [9].

Input waveguide and horn throat section

The dimensions of the input sections of a corrugated horn are a compromise between low VSWR and suppression of unwanted high order modes. A large input waveguide produces the lowest VSWR, but if the feed is operated at frequencies above the cutoff frequency of the TE_{12} mode in circular waveguide the designer must be careful not to excite this mode.

Terzuoli, et al. [9] considered the problem of matching from waveguide to a flared corrugated horn. They found that a considerably better match was obtained with a smooth transition from waveguide to flare than with a direct angular transition. The minimum length over which this transition should occur is about 0.8 λ at the lowest frequency.

Terzuoli, et al. [10] also looked at the problem of coupling the RF energy between the smooth and corrugated parts of the horn. They and other workers agree that it is best not to start the corrugations too close to the waveguide to horn transition and to begin with slots nearly $\lambda/2$ deep and taper into $\lambda/4$ depth slots. However, the first slot must occur at a point in the horn where the diameter is less than $4\lambda/\pi$ at the highest operating frequency to prevent excitation of the EH_{12} mode (Thomas [11]). What would normally have been the first three slots were omitted in the 11.5-15.5 GHz horn, and the first slot was made 0.4 λ deep at 15.5 GHz. A better match at the low frequency end could have been obtained if the first slot were closer to 0.5 λ deep and the second slot were 0.4 λ deep at 15.5 GHz. A comparison between the return loss from

an angular transition with equal depth slots and a smooth transition with a deeper first slot is shown in the next section.

Dimensions and Test Results

The 11.5-15.5 GHz horn was designed to have an 11 dB taper at the edge of the 140-foot Cassegrain secondary (half angle = 7.14). The aperture diameter and distance from the aperture to the cone apex are 38 cm and 120 cm, respectively, and the overall length of the horn from the input waveguide flange to the aperture is 114.3 cm or 45 inches. Figure 1 is a photograph of the completed horn. The first 15 cm on the small end is electroformed copper in two sections to allow experimentation with the throat section without remaking the whole first section. The remaining part of the horn was machined from 6" thick aluminum plate stock. There are six 5.81 (14.75 cm) and one 3.87 (9.83 cm) long aluminum sections beyond the electroformed part.

Figure 2 is a drawing of the two throat sections tried. The longer tapered throat (2b) is the one finally adopted. Except for the first, all slots are 0.63 cm deep and 0.25 cm wide, and the vanes between the slots are 0.25 cm thick. This makes the slots $\lambda/4$ deep at 11.9 GHz and spaced 4 per wavelength at 15 GHz. The input waveguide diameter of 1.96 cm produces a TE_{12} cutoff frequency of 14.9 GHz. The frequency range of the horn could be extended to about 16.5 GHz by adding another slot closer to the horn apex, and the low frequency return loss might be improved by making the first and second slots deeper. Figure 3 shows a suggestion for a new throat section.

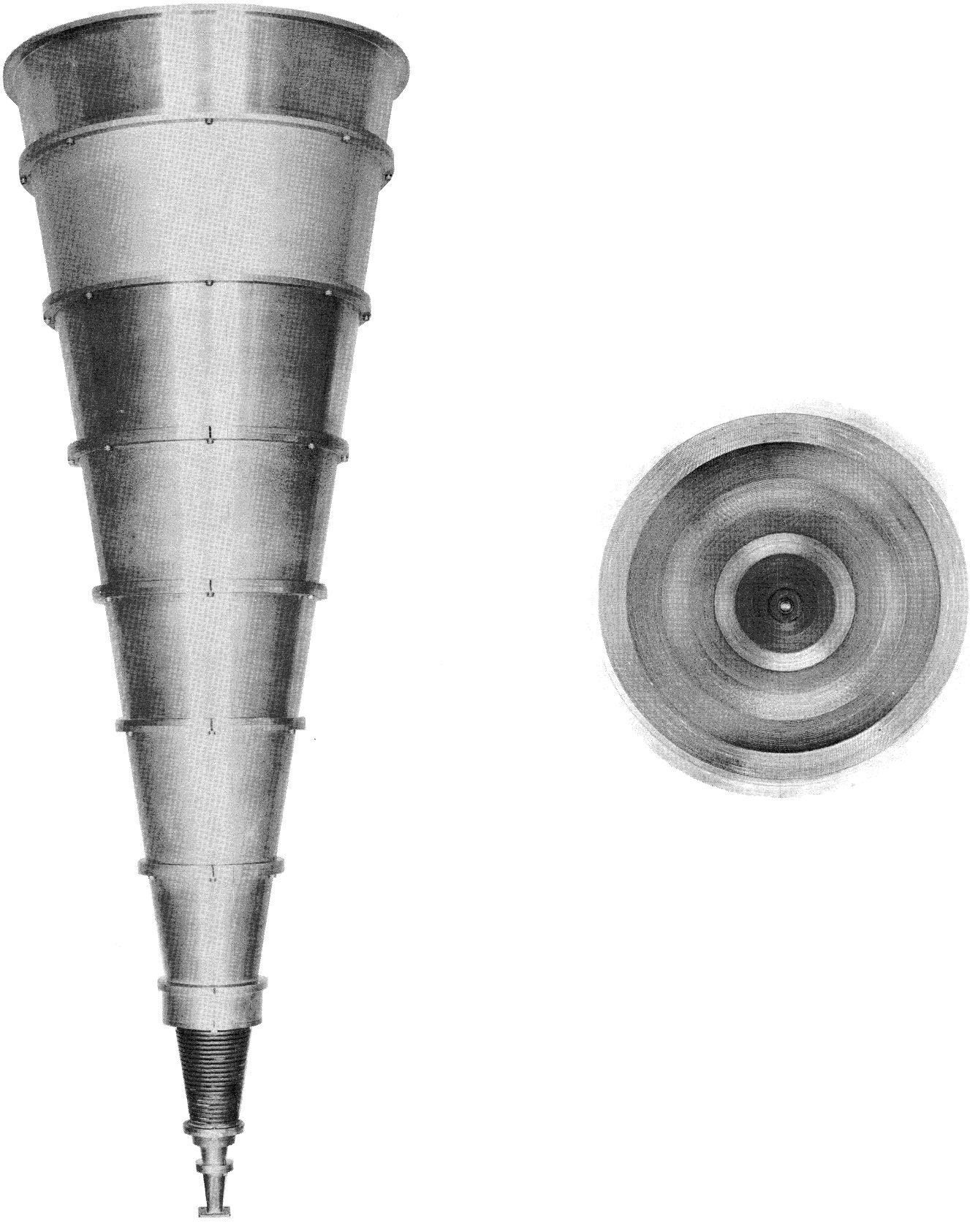

Figure 1. Completed feed. The first 15 cm is electroformed copper and the rest is machined aluminum.

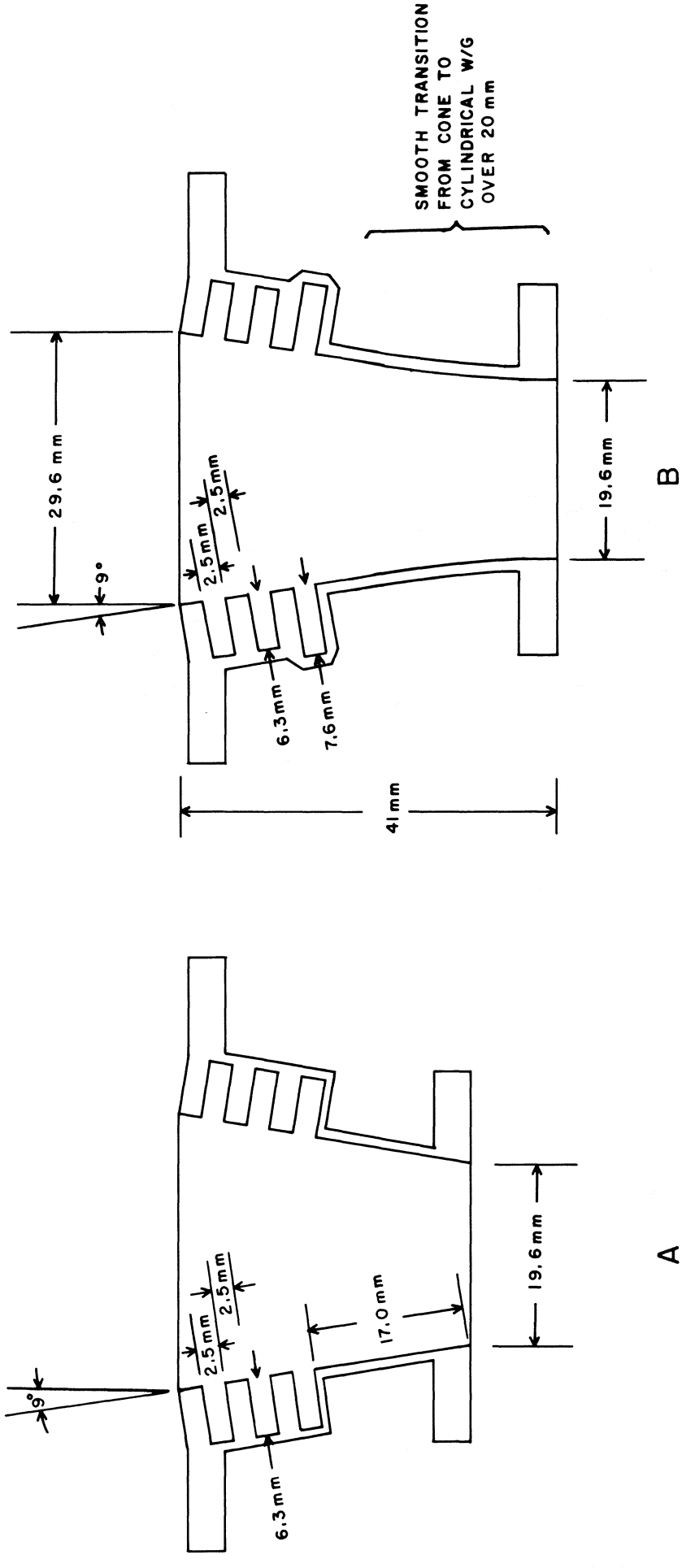

Figure 2. Two horn throat sections measured for return loss. Section b was adopted.

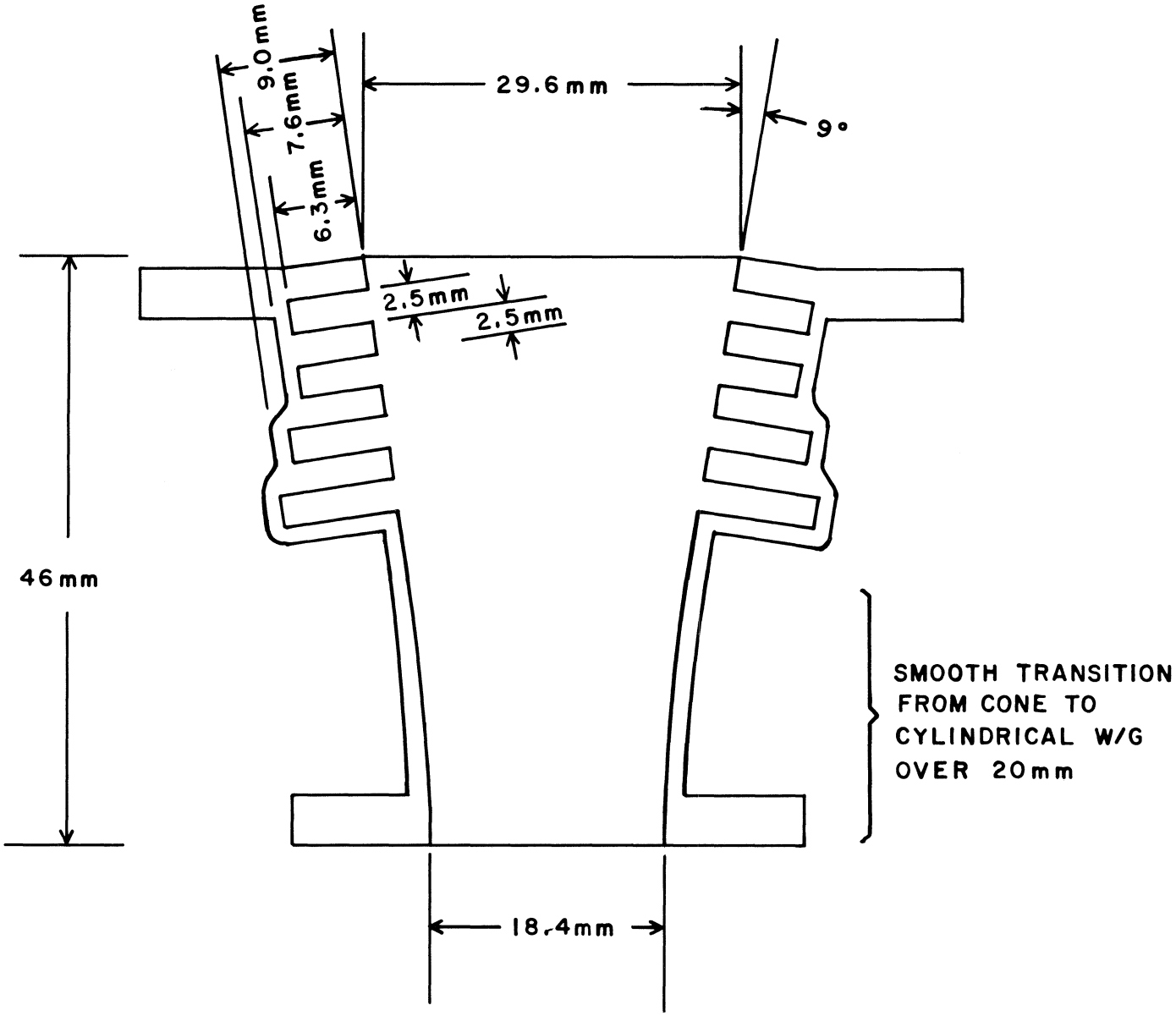

Figure 3. Suggestion for a new throat section to extend the frequency coverage of the horn.

Return loss

Figure 4 shows the return loss as a function of frequency for the two horn throats illustrated in Figure 2. A considerable improvement is seen when the transition between waveguide and the horn is done smoothly and the first slot is cut deeper, but I do not know which of the changes was responsible for the largest portion of the improvement.

The return loss measurements were made with only the first 15 cm length of horn since the rest of the horn has relatively little effect. In fact, just the throat sections themselves produced nearly the same results as the 15 cm horn. The measurements were made with a Pacific Measurements, Inc., Model 1038 system and WR 62 rectangular waveguide directional couplers. A special 12.5 cm long rectangular to circular waveguide transition was electroformed for the tests, and its reflection coefficient was measured to be at least -32 dB but more typically -34 to -40 dB across the frequency range of interest.

Radiation patterns

Linear polarization radiation patterns were measured in the E and H planes at a number of frequencies between 11 and 17.5 GHz, and the results are shown in Figures 5 through 8. Patterns outside of the intended frequency range are shown to illustrate one of the factors limiting the bandwidth of the feed. The E-plane patterns (Figure 5) are most affected by surface waves on the horn walls and higher order modes in the horn throat. For reference, the 14 GHz pattern is superimposed as a dashed line on the patterns at other frequencies. The H-plane patterns are similarly plotted in Figure 6, and the E and H-plane patterns are plotted together in Figure 7.

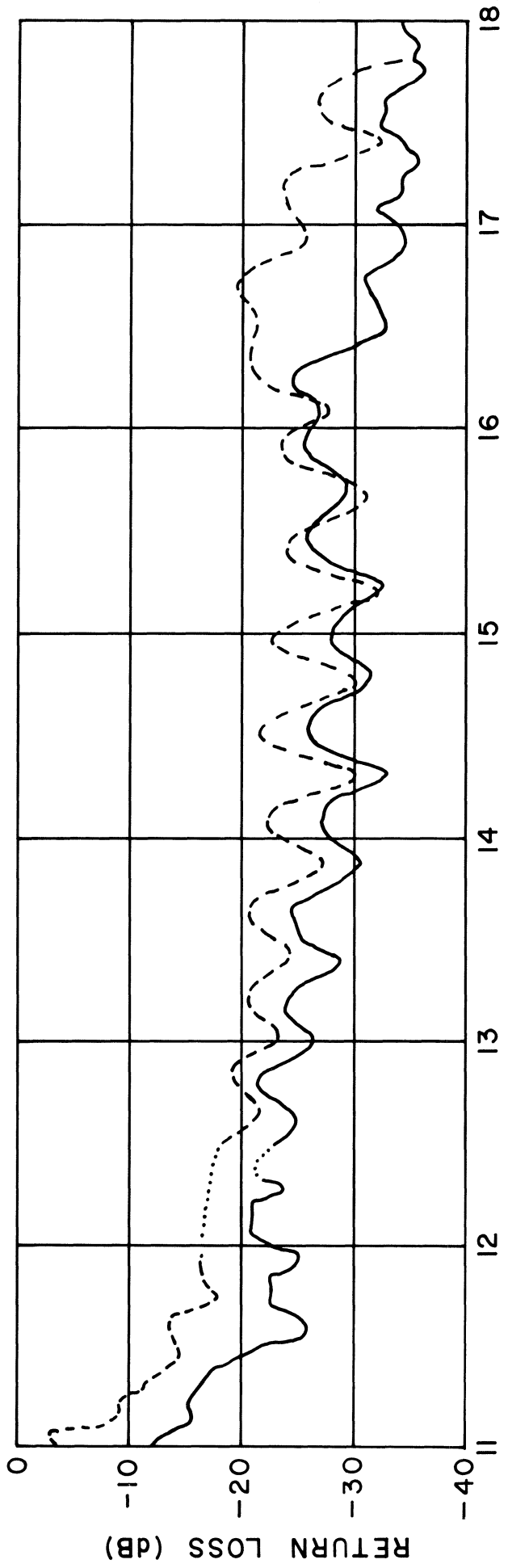

Figure 4. Return loss as a function of frequency for throat sections in Figures 2a (dashed) and 2b (solid).

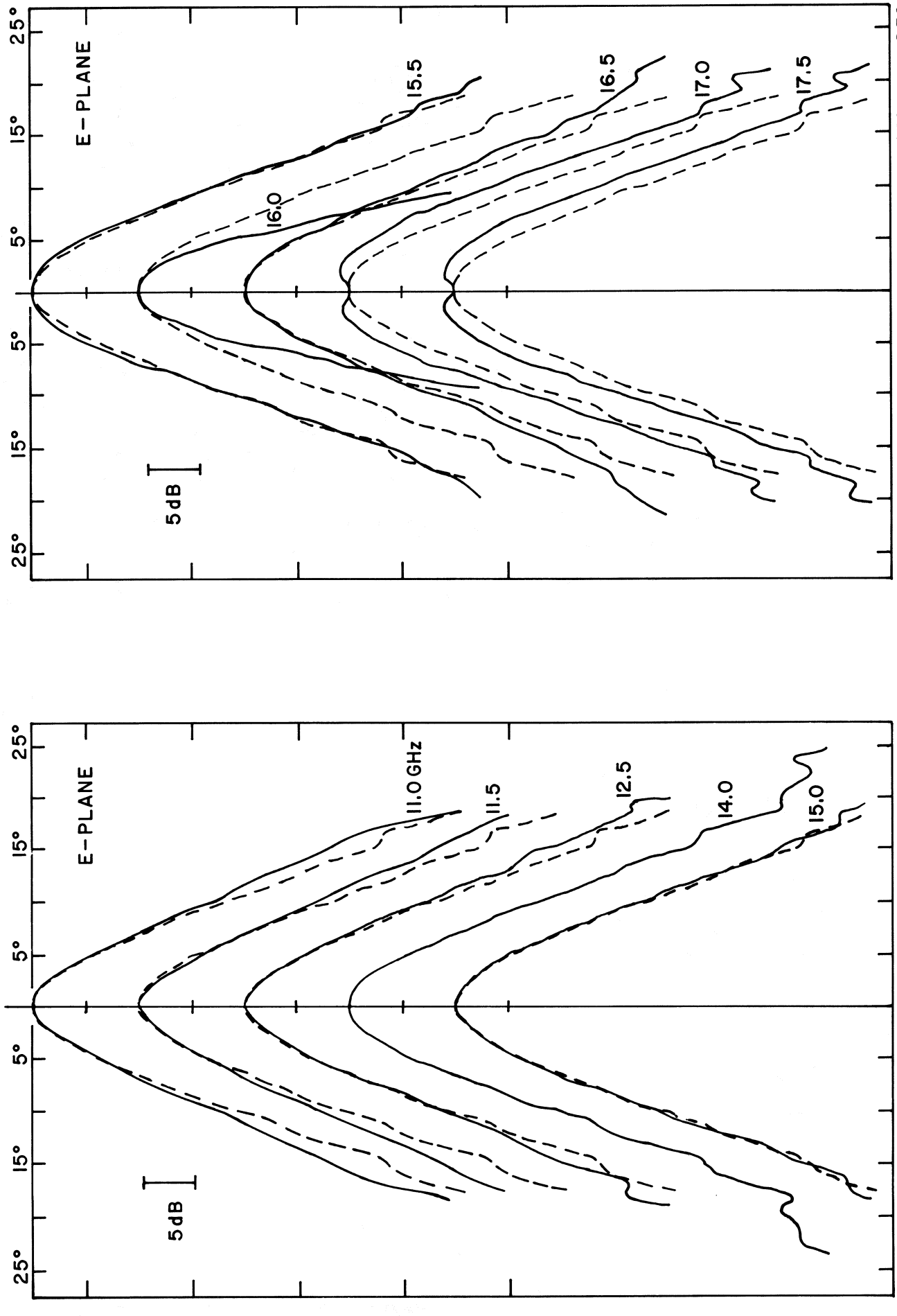

Figure 5. E-plane patterns of the 11.5-15.5 GHz horn at a number of frequencies. The 14.0 GHz curve is superimposed on the other curves as a dashed line for comparison.

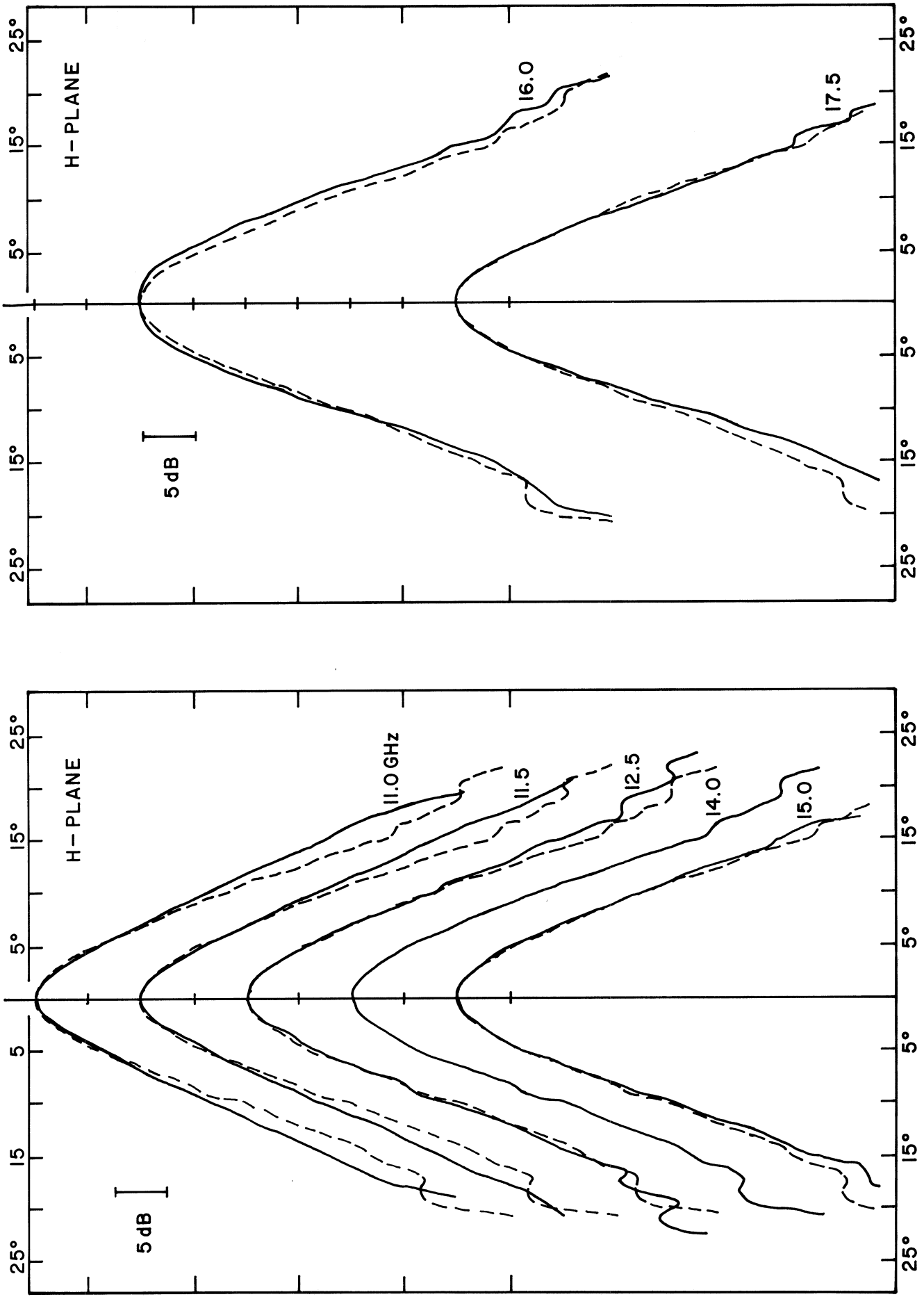

Figure 6. H-plane patterns of the 11.5-15.5 GHz horn at a number of frequencies. The 14.0 GHz curve is superimposed on the other curves as a dashed line for comparison.

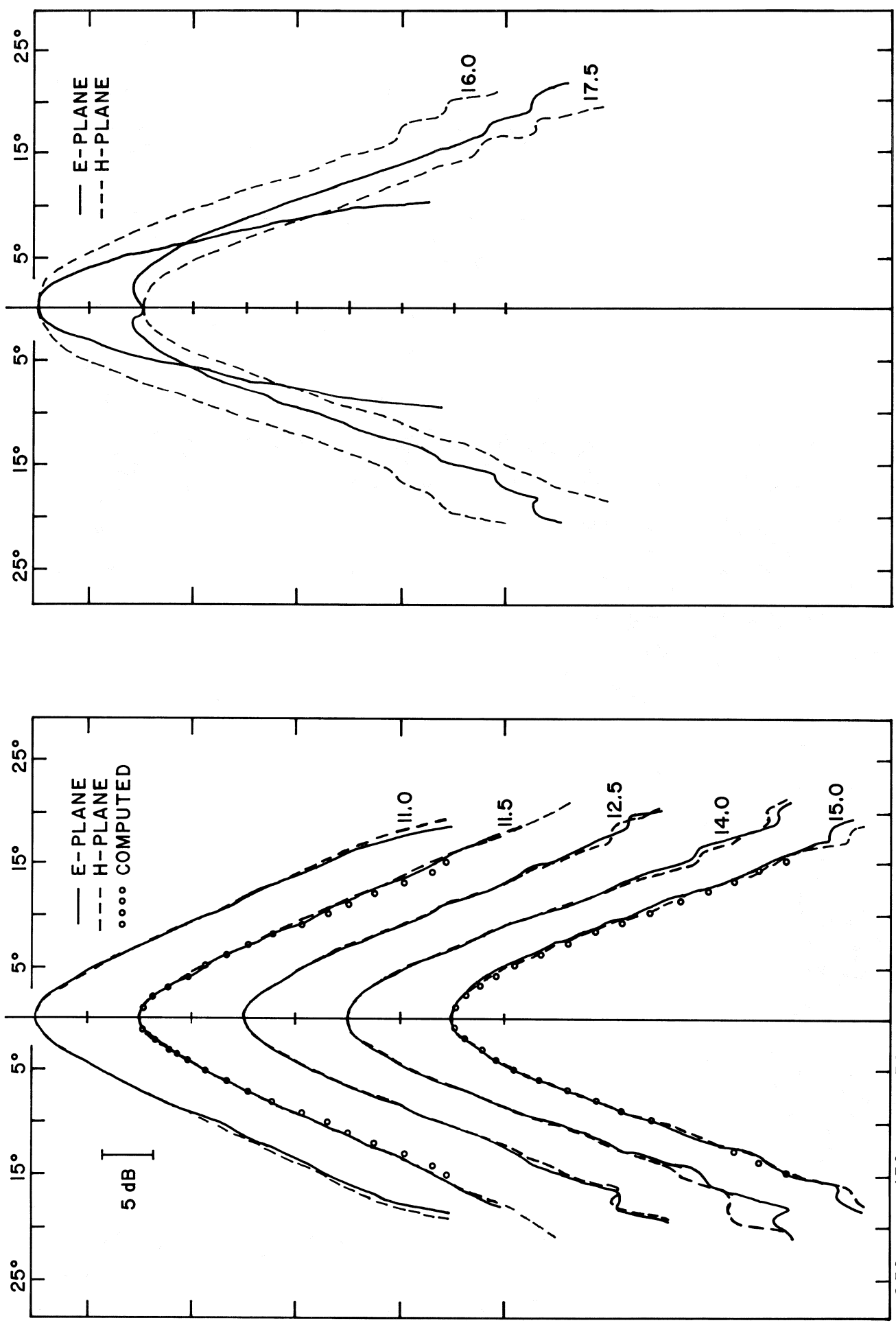

Figure 7. Comparison of E (solid) and H (dashed) plane patterns of the 11.5-15.5 GHz feed. Computed patterns are shown as points on the 11.5 and 15.5 GHz curves.

The corrugation slots are $\lambda/4$ deep at 11.9 GHz, but they are still quite effective at 11.0 GHz since the E and H-plane patterns are well matched at this frequency. It is obvious from the E-plane patterns that the EH_{12} mode becomes important above 15.5 GHz. This is just what is expected since the first slot occurs at a horn diameter of $4\lambda/\pi$ at 15.33 GHz. The rapid change in E-plane pattern shape between 15.5 and 17 GHz is due to the changing phase between the HE_{11} and EH_{12} modes.

The excellent pattern circularity which is characteristic of corrugated horns is shown in Figure 7. The E and H-plane patterns differ by less than a few tenths of a dB to more than 25 dB below the beam peak in the useful frequency range. The pattern equations will be given in the last section, but computed patterns at 11.5 and 15 GHz are shown in Figure 7 where good agreement with the measured results can be seen.

Figure 8 shows the feed pattern beamwidths as a function of frequency for a number of levels relative to the beam center. Figure 9b is a plot of the illumination at the edge of the 140-foot Cassegrain subreflector, and Figure 9a shows the spillover efficiency of the feed as a function of frequency.

The cross polarization response of the feed was measured in the E-plane at 13, 15, and 16 GHz and was found to be more than 30 dB below the intended linear polarization at 13 and 15 GHz. At 16 GHz the cross polarization rose to -24 dB about 3° away from the beam peak.

Phase patterns were measured in the E-plane at 11.5, 14.0, 16.0, and 17.5 GHz. The phase is well behaved to about the 17 dB point on the amplitude pattern and follows the predicted curves (Figure 13) considerably beyond that point. Over the angle subtended by the subreflector there is a well defined phase center with a residual phase error of less than $\pm$ 5° in the useful frequency range, but beyond the 17 dB point the deviation from a spherical wavefront is rather sharp,

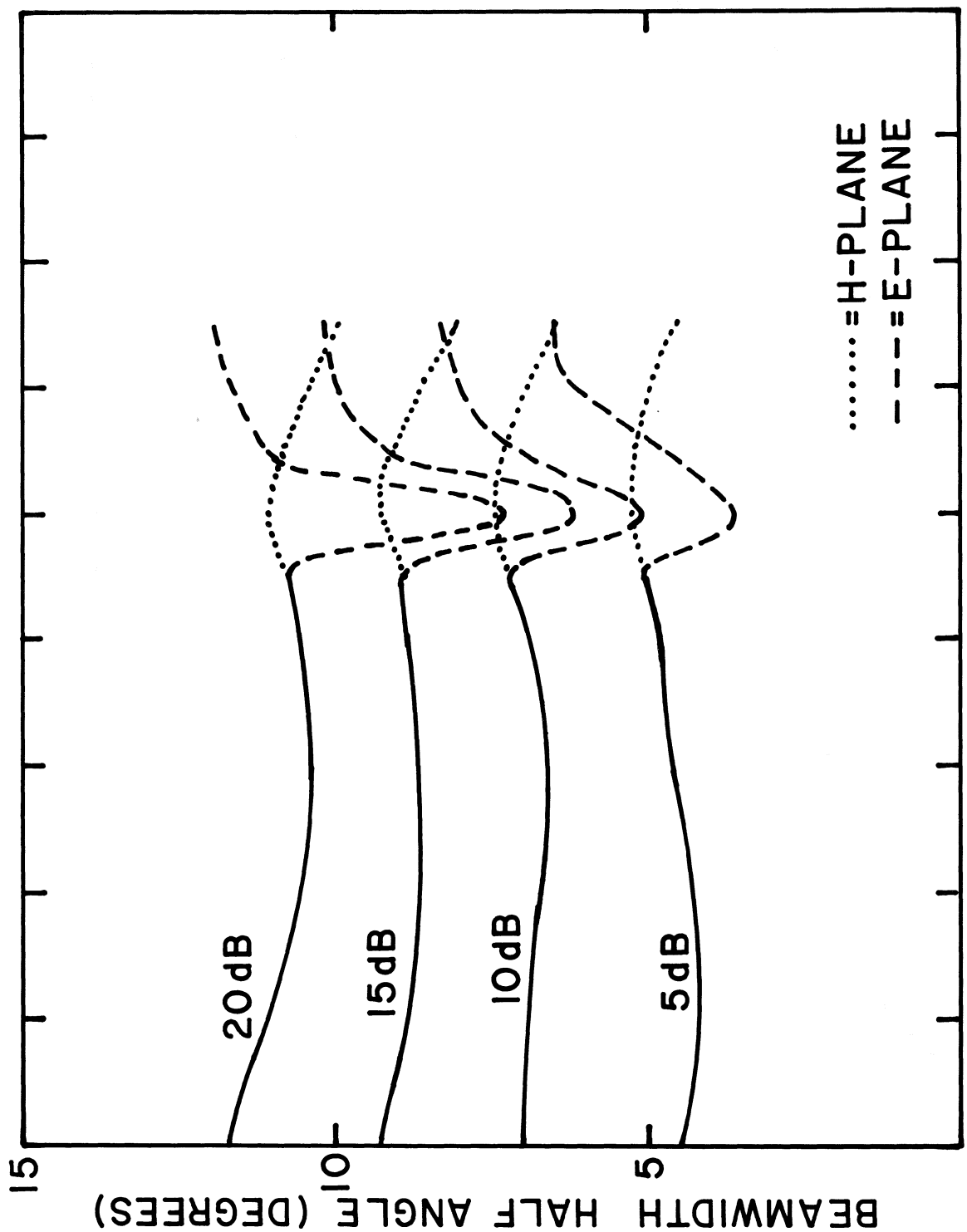

Figure 8. Beamwidth of 11.5-15.5 GHz horn as a function of frequency for four levels relative to beam peak.

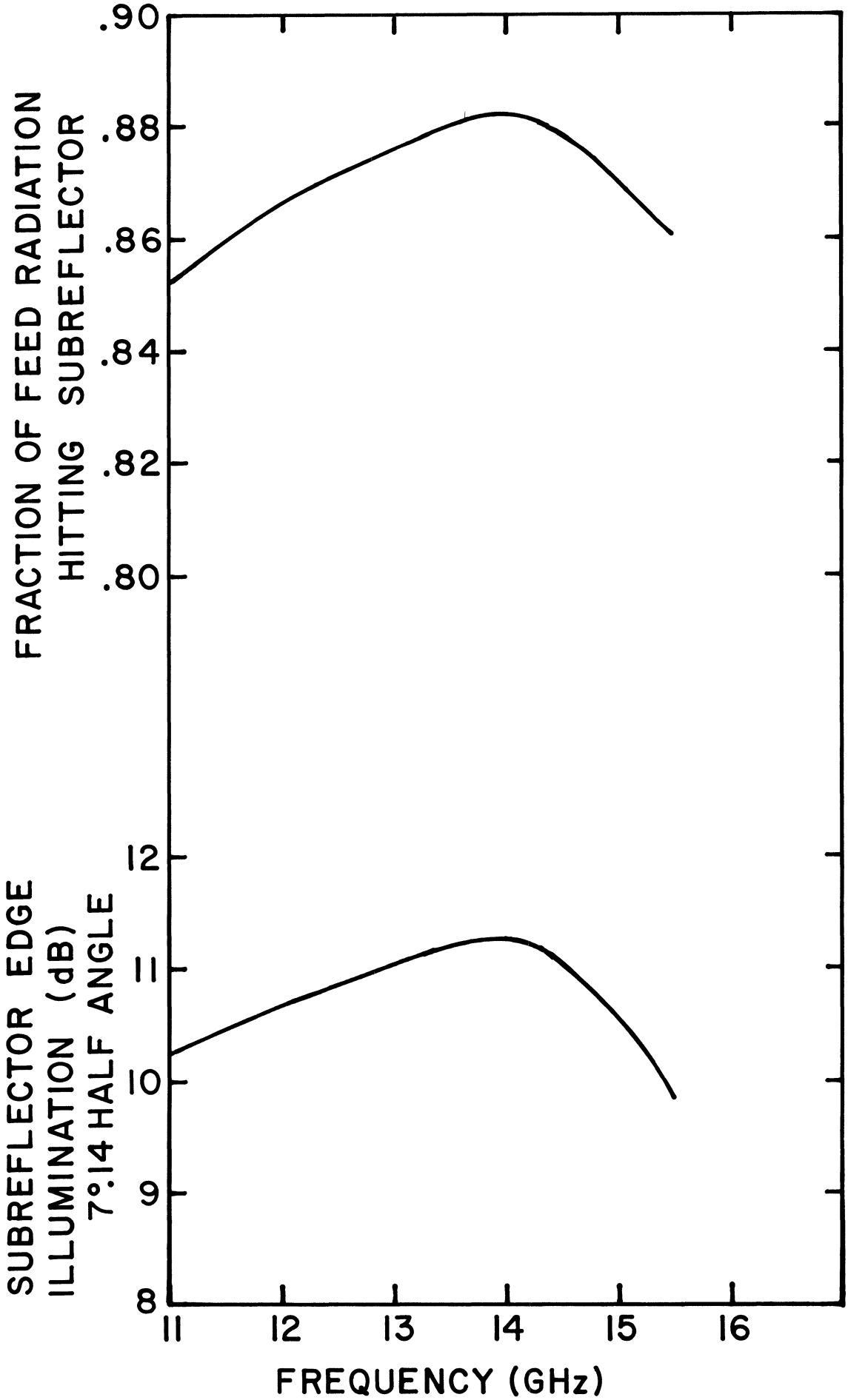

Figure 9. Feed spillover efficiency with the 140-foot subreflector (a) and subreflector edge illumination (b).

and the phase error exceeds 90° at about 35 dB below the beam peak. Although the feed is not very useful above 15.5 GHz the phase pattern up to 17.5 GHz is not far from what is expected for a single mode feed. As predicted the phase center position is a function of frequency (Figure 10); however, if the feed were properly focused at 11.5 GHz the loss in telescope aperture efficiency at 15.5 GHz due to being 17 cm out of focus would be less than 2%.

Telescope Aperture Efficiency and Spillover

Figure 11 shows the Cassegrain subreflector diffraction patterns computed at 12 and 15 GHz using the feed radiation patterns in Figure 7. The diffraction patterns are based on a symmetrical subreflector, but they are not significantly different for a moderately asymmetrical subreflector such as the one used on the 140-foot.

Aperture efficiencies, spillover and scattered ground radiation temperature were computed from the patterns in Figure 11, and the results are tabulated in Table 1. Efficiency loss due to phase ripples on the order of $\pm$ 15° near the edge of the subreflector diffraction pattern are not included, but this causes a total loss of less than 1%. Measured efficiencies on the NRAO telescopes have generally been lower than predicted by a factor of about 0.8 for unknown reasons so the total efficiencies in Table 1 are probably too optimistic by this amount.

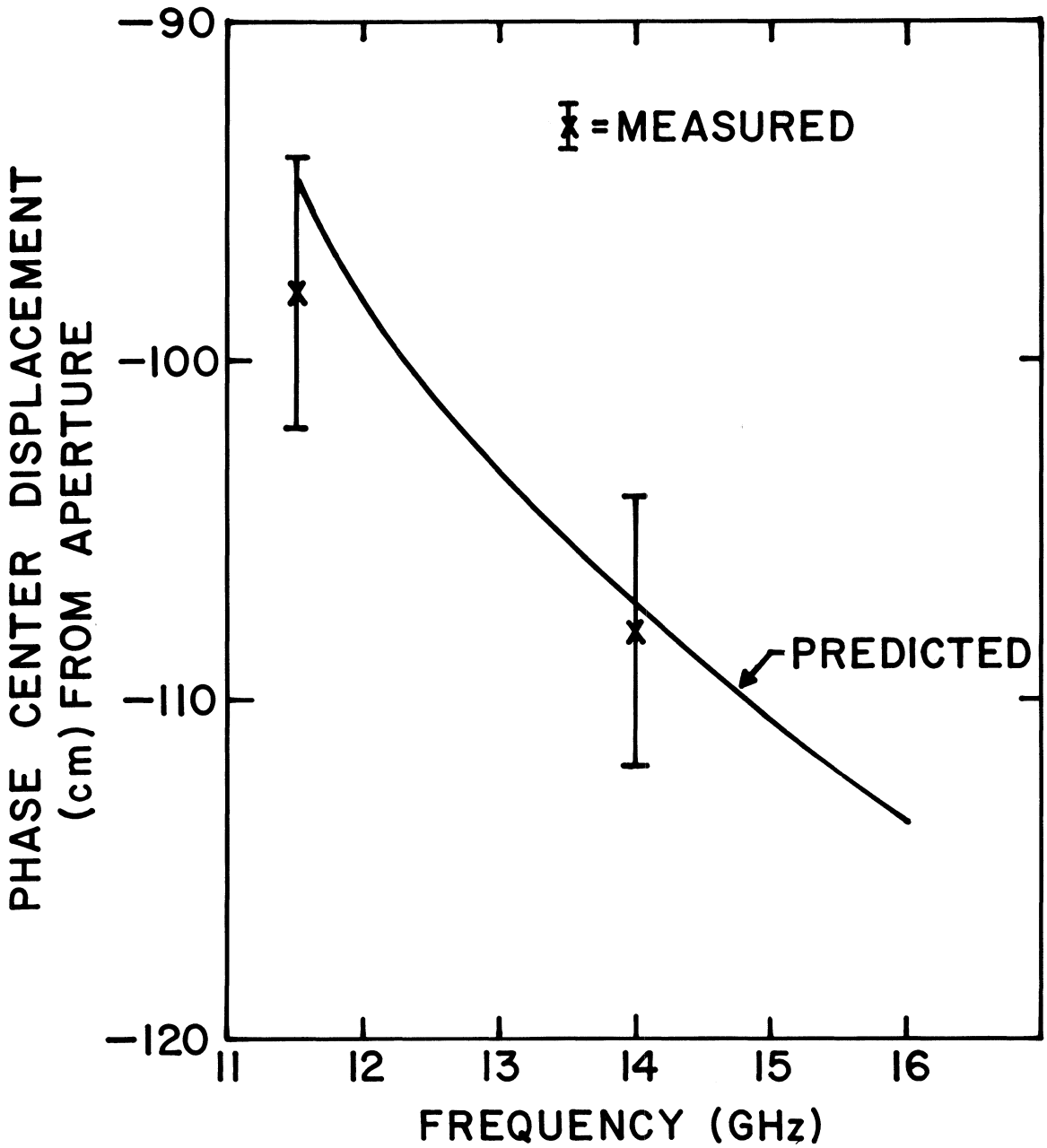

Figure 10. Phase center distance from the aperture of the 11.5-15.5 GHz feed. More negative distances are in the direction of the feed apex.

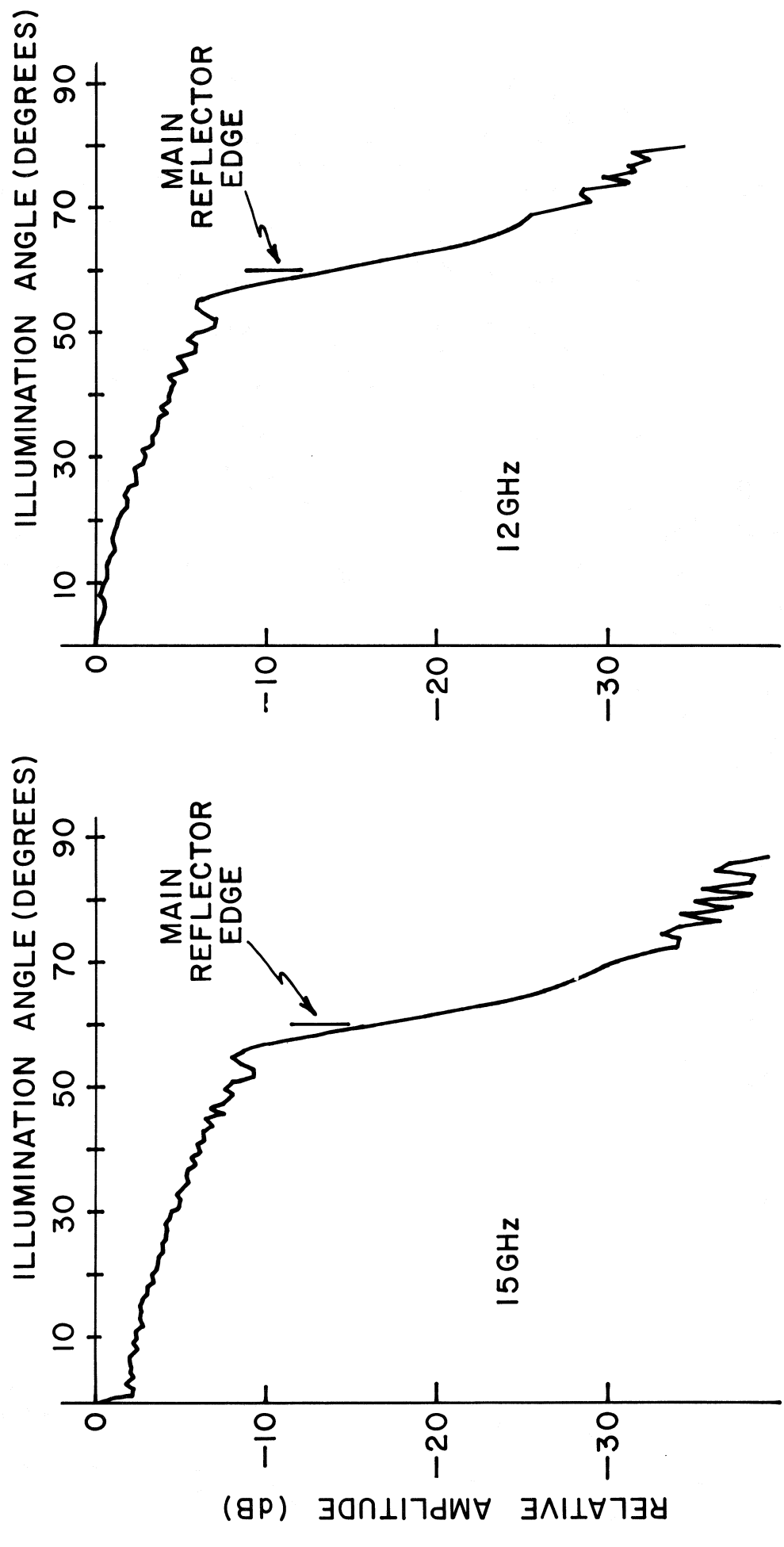

Figure 11. 140-foot subreflector diffraction patterns when illuminated by the 11.5-15.5 GHz feed at 12 and 15 GHz.

TABLE 1

Computed 140-foot telescope parameters with the 11.5 to 15.5 GHz corrugated horn.

	12 GHz	15 GHz
Feed pattern spillover efficiency	0.866	0.870
Subreflector pattern spillover efficiency ...	0.990	0.993
Main aperture taper efficiency	0.872	0.866
Blockage loss	0.880	0.880
Surface error loss*	0.85	0.77
Total efficiency	0.56	0.51
Spillover temperature	1.9 K	1.5 K
Scattered ground radiation temperature	3.1	3.1
Total temperature	5.0 K	4.6 K

* Assumes 50% surface error loss at 22 GHz.

Calculator Programs for Radiation Patterns

The complex far field radiation pattern of a conical corrugated horn is given by Loefer, et al. [4] as

$$E(\Theta) = [1 + \cos \Theta] \int_0^1 J_0(\alpha_1 r)\, J_0(P_{01} r)\, e^{-jvr^2} r\, dr \qquad (2)$$

where

$$\alpha_1 = \frac{2\pi a \sin \Theta}{\lambda} \qquad (3)$$

$$v = \frac{\pi a^2}{\lambda L} \qquad (4)$$

P_{01} = 2.405 (first zero of J_0)

a = horn aperture radius

L = horn axial length

J_0 = Bessel function of the first kind, order zero

and Θ = far field pattern coordinate measured from the horn axis.

The term $J_0(P_{01} r)$ is the aperture field strength as a function of the normalized radius, r, and $J_0(\alpha_1 r)$ is the far field voltage pattern of a single annulus in the aperture plane. The value v has the same origin as equation (1). Equation (2) can be divided into real and imaginary parts:

$$E(\Theta) = E_R - j\, E_I \qquad (5)$$

where

$$E_R = [1 + \cos \Theta] \int_0^1 J_0(\alpha_1 r)\, J_0(P_{01} r) \cos (vr^2)\, r\, dr \qquad (6a)$$

and

$$E_I = [1 + \cos \Theta] \int_0^1 J_0(\alpha_1 r)\, J_0(P_{01} r) \sin (vr^2)\, r\, dr \qquad (6b)$$

The far field amplitude pattern is then

$$E(\Theta) = (E_R^2 + E_I^2)^{1/2} \tag{7}$$

and the phase pattern is

$$\phi(\Theta) = \tan^{-1} \frac{E_I}{E_R} \tag{8}$$

The phase center is the point around which the feed can be rotated to keep the phase at a far field point constant over the central portion of the beam. If $\underline{\ell}$ is the distance of the phase center from the horn aperture then

$$\frac{2\pi\ell}{\lambda} (1 - \cos \Theta) \simeq \phi(\Theta) \tag{9}$$

where $\phi(\Theta)$ is in radians. This equality will not be exact over the full range of Θ of interest with a single $\underline{\ell}$ since the wavefront is not perfectly spherical. The calculator program determines $\underline{\ell}$ by satisfying equation (9) at $\Theta = 0°$ and $\Theta = 5.865$.

The amplitude and phase pattern calculations were written as two separate programs although there is not much difference between them. The programs are listed in Tables 2 and 3. The subroutine "besl" will compute J_0 and J_1 although only J_0 is used here. The input parameters for both programs are:

1. "PLOT #". If 1 is entered the axes are plotted and the horn parameters are printed on the X-Y plot. If any number greater than 1 is entered only the computed curve is plotted, and the axes are not duplicated. This permits putting more than one curve on a plot.

2. "Aperture Radius" in cm.

3. "Horn Axial Length" in cm.

4. "Wavelength" in cm.

The output from the amplitude program is shown in Figure 12, where vertical axis tick marks are at 5 dB intervals and horizontal axis ticks are at 1° intervals. A vertical hash mark denotes the edge of the 140-foot subreflector at 7.°14. The value D/W is the phase difference in wavelengths between the center and edge of the horn aperture field. The values of D/W in wavelengths, spillover efficiency in % and the horn flare angle in degrees are also displayed on the calculator LED's. The individual curves in Figure 12 were identified and the different spillover efficiencies were put on the plot by hand.

Figure 13 shows the phase program output. In this case the vertical axis ticks are at 20° intervals of phase. The idealized spherical phase pattern given by the left hand side of equation (9) is subtracted from the computed horn phase pattern, $\phi(\Theta)$, so, by definition, the plotted curve will pass through the horizontal axis at $\Theta = 0°$, and 5.°865.

Acknowledgements

All of the machine work for the horn was very ably performed by Wendell Monk and Boyd Wright in the Green Bank shop under the supervision of Martin Barkley. The electroforming was done in the Charlottesville lab by John Lichtenberger.

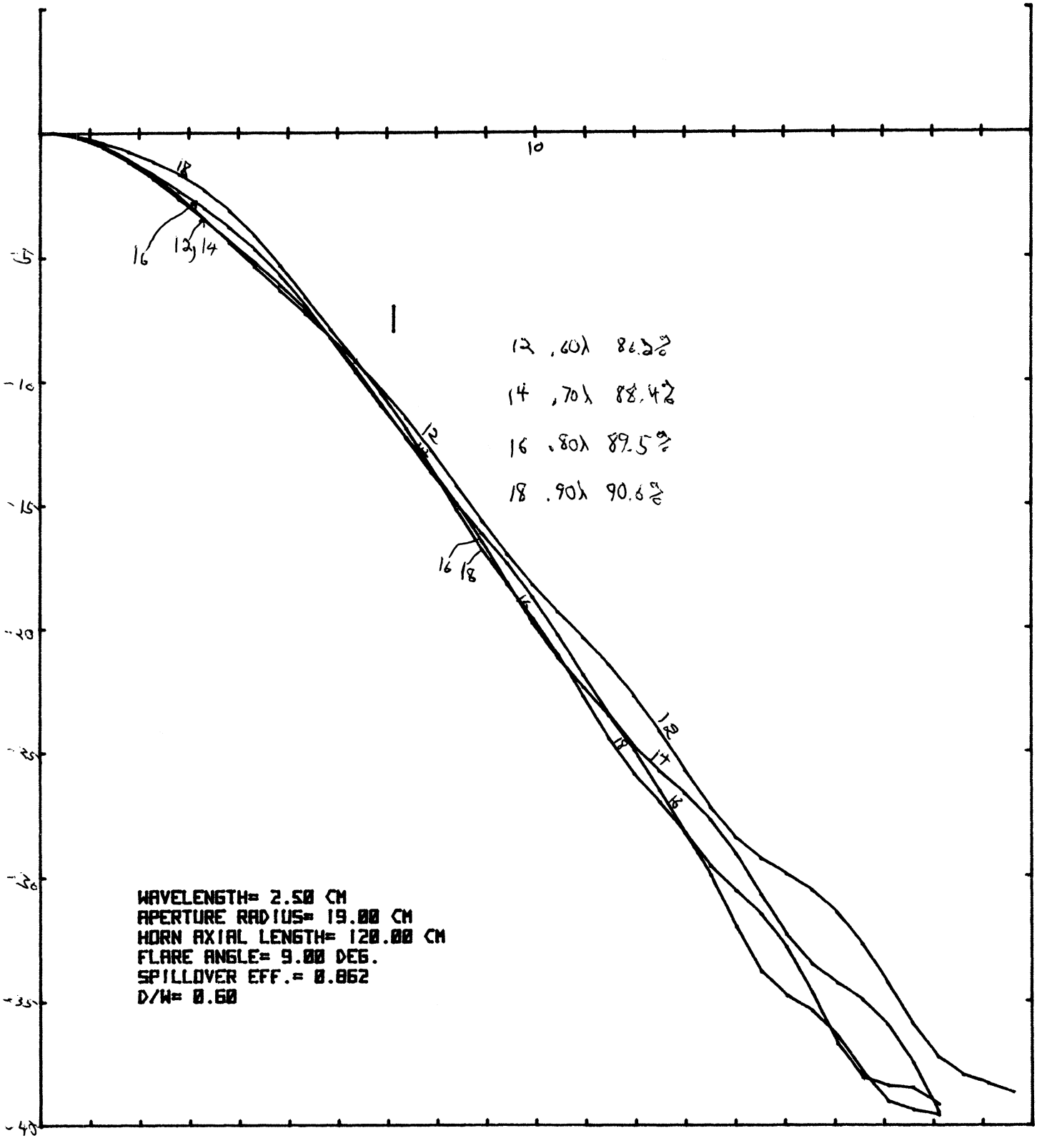

Figure 12. Output of 9825A calculator amplitude program for feed radiation pattern prediction.

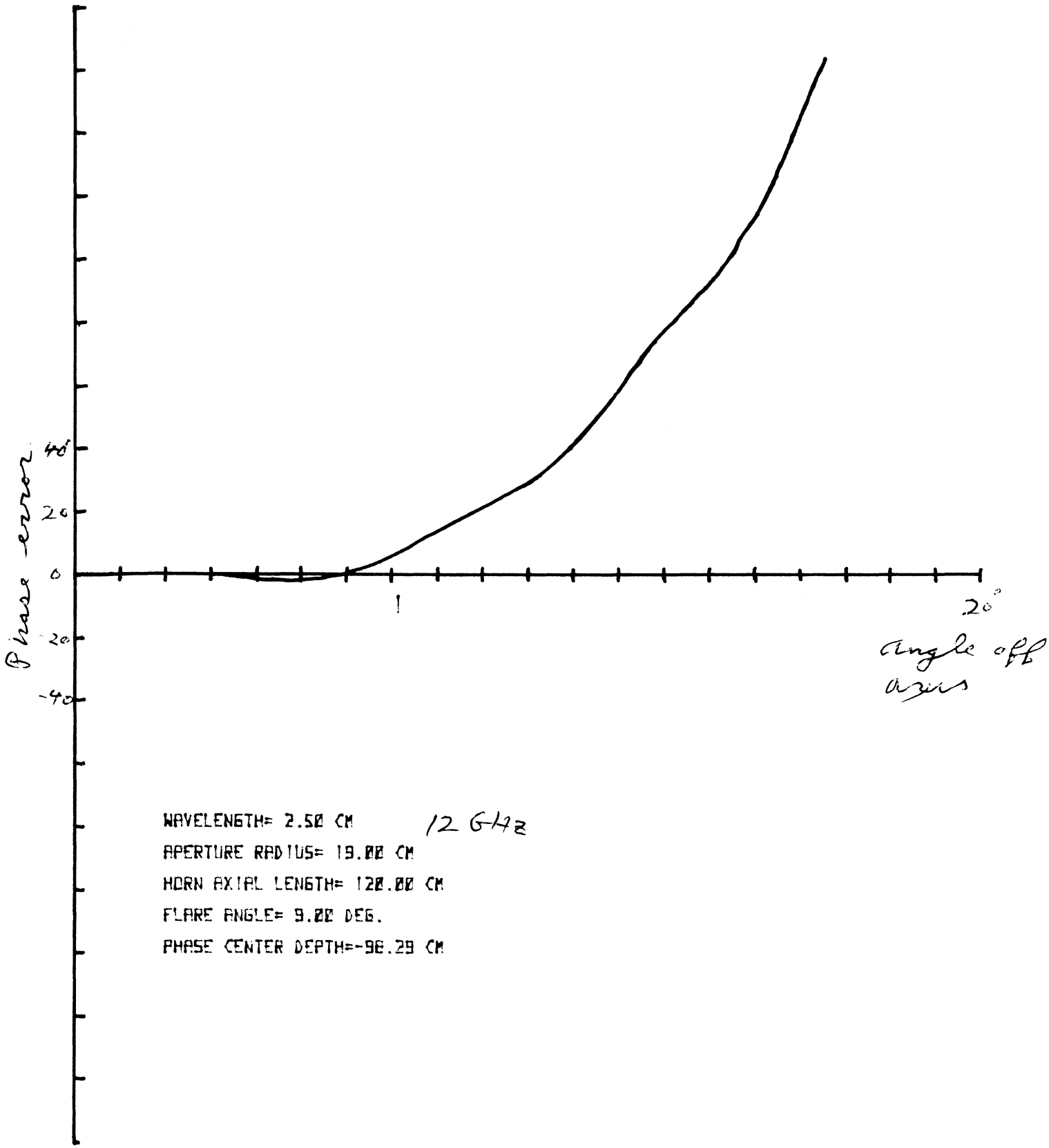

Figure 13. Output of 9825A calculator phase pattern program for feed radiation pattern prediction.

TABLE 2

AMPLITUDE PROGRAM

```
00: fmt 1:2f6.1;
    dim Z[20]
01: ent "PLOT
    #?",N
02: ent "Aperture
    Radius?",A
03: ent "Horn
    Axial Length?",
    L
04: ent "Wavelens
    th?",W
05: gcl 0,20,-40,
    5;csiz 1,1,1.3,
    0
06: if N>1;sto +2
07: axe 0,0,1,5;
    aye 20,-40,1,5;
    csiz 1,1.2,.8,0
08: plt 0,0,1
09: 180A↑2/WL→V
10: 0→C→D→K
11: for R=.025
    to .975 by .05
12: K+1→K
13: 'besl'(2.405
    R)→Z[K]
14: next R
15: for T=.51
    to 20 by 1.02
16: 2πAsin(T)/
    W→B
17: 0→X→Y→F
18: for R=.025
    to .975 by .05
19: K+1→K
20: 'besl'(BR,
    0)↑2→U
21: (R↑2→U
22: X+.05R0Z[K]c
    os(U)→X
23: Y+.05R0Z[K]s
    in(U)→Y
24: next R
25: 20log((1+
    cos(T))/(X↑2+
    Y↑2))→E
26: C+Tan↑(.1E)→
    C
27: if T<7.14;
    goto 0
28: if T=.51;F→F
29: E-F→E
30: plt T,E,2
31: next T
32: L(1/cos(atn(
    A/L))-1)/W→X
33: fxd 2;dsp X,
    "wl ",100D/C,
    "% ",atn(A/L),
    "deg"
34: if N>1;pen;
    stp
35: plt 2,-31,1;
    fxd 2
36: lbl "Wavelen
    gth=",W," cm"
37: plt 2,-31.8,
    1
38: lbl "Apertur
    e Radius=",A,"
    cm"
39: plt 2,-32.6,
    1
40: lbl "Horn
    axial length=",
    L," cm"
41: plt 2,-33.4,
    1
42: lbl "Flare
    angle=",atn(A/
    L)," Deg.
43: fxd 3;plt 2,
    -34.2,1
44: lbl "Spillov
    er eff.=",D/C
45: plt 2,-35,1;
    fxd 2
46: lbl "d/w=",X
47: plt 7.14,-
    10.5,1;plt 7.14
    ,-11.5,2
48: plt 6.64,-
    11,1;plt 7.64,-
    11,2
49: pen;stp
50: "besl":if
    p2=1;goto +18
51: if p1>10;
    goto +7
52: (p1/2)↑2→p3;
    1→p4;0→p5;1→p6
53: (p1/2)↑2→p3;
    1→p4;0→p5;1→p6
54: p5+1→p5;-
    p4p3/p5↑2→p7
55: if abs(p7-
    p4)>1e-6;p6+
    p7→p6;p7→p4;
    goto -1
56: if p2=2;goto
    +12
57: ret p6
58: 0p1→p3;1→p4;
    -1→p5;0→p6→p7
59: p6+p4→p6
60: p5+2→p5
61: -2p4p5↑2/
    (p5+1)p3→p8;p7+
    p8→p7
62: p5+2→p5;2p8p
    5↑2/(p5+1)p3→p4
63: if abs(p4-
    p8)>1e-6;goto -4
64: rad;p1-.7853
    98→p9
65: r(.63662/
    p1)(p6cos(p9)-
    p7sin(p9))→p6
66: if p2=2;goto
    +2
67: ret p6
68: if p1>10;
    goto +7
69: if p1=0;ret
    0
70: (p1/2)↑2→p3;
    0→p5;p1/2→p4→p8
71: p5+1→p5;-
    p3p4/p5(p5+1)→p
    7
72: if abs(p7-
    p4)>1e-6;p7→p4;
    p7+p8→p8;goto -1
73: if p2=2;ret
    2p8/p1-p6
74: ret p8
75: 0→p5;1/8p1→p
    3;1→p4;1→p8;
    0→p9
76: p5+1→p5;-
    p4p3(2p5-3)(2p5
    +1)/p5→p4
77: p4+p9→p9
78: p5+1→p5;p4p3
    (2p5-3)(2p5+1)/
    p5→p7
79: if abs(p7-
    p4)>1e-6;p7→p4;
    p7+p8→p8;goto -3
80: rad;r(.63662
    /p1)(p8cos(p1-
    .75π)-p9sin(p1-
    .75π))→p8
81: if p2=2;ret
    2p8/p1-p6
82: ret p8
*6722
```

TABLE 3

PHASE PROGRAM

```
0: fmt 1;2f6.1;
 3;0→r0;dim Z[20
 1
1: ent "PLOT
 #?";N
2: ent "Aperture
  Radius?";A
3: ent "Horn
 Axial Length?",
 L
4: ent "Wavelen
 th?";W
5: scl 0; ,-
 100,100;csiz 1,
 1;1.3,0
6: if N>1;sto +2
7: plt 0,0,1
 : 180A↑2/WL→V
10: 0→C→D→I→K
11: for R=.025
 to .975 by .05
12: K+1→K
13: "Besl"(2.405
 R);→Z[K]
14: next R
15: for T=.255
 to 20 by .5;
16: ZmAsin(T)/
 W→B
17: 0→X→Y→K;I+
 1→I
18: for R=.025
 to .975 by .05
19: K+1→K
20: "Besl"(BR,
 0);→W;deg
21: VR↑2→U
22: X+.05R*Z[K]c
 os(U)→X
23: Y+.05R*Z[K]s
 in(U)→Y
24: next R
25: atn(abs(Y/
 X))→r]
26: if X>0 and
 Y>0;sto +4
27: if X<0 and
 Y>0;180-r]→r];
 sto +3
28: if X<0 and
 Y<0;180+r]→r]
 sto +2
29: if X>0 and
 Y<0;360-r]→r]
30: if r]>r[]-
 1];r]-360→r]
31: dsp T,r]
32: next T
33: for J=1 to
 1 by -1;rJ-r1→r
 J;next J
34: r12/.005235→
 X
35: for J=1 to
 I;rJ-X(1-cos(.5
 1J-.255))→rJ
36: if rJ<-180;
 rJ+360→rJ
37: if rJ>180;
 rJ-360→rJ
38: next J
39: 0→I
40: dsp "Phase
 center depth=",
 XW/360
41: for T=.255
 to 20 by .5;I+
 1→I
42: plt T,r],2;
 next T
43: if N>1;ptyp;
 stp
44: plt 2,-80,1;
 fxd 2
45: lbl "Wavelen
 gth=",W," cm"
46: plt 2,-90,1
47: lbl "Apertur
 e Radius=",A,"
 cm"
48: plt 2,-100,1
49: lbl "Horn
 axial length=",
 L," cm"
50: plt 2,-110,1
51: lbl "Flare
 angle=",atn(A/
 L)," Deg."
52: plt 2,-120;
 fxd 2
53: lbl "Phase
 center depth=",
 XW/360," cm"
54: plt 7.14,-7;
 1;plt 7.14,-12;
 2
55: penstp
56: "basl":if
 p2=1;sto +18
57: if p1>10;
 sto +7
58: (p1/2)↑2→p3;
 1→p4;0→p5;1→p6
59: (p1/2)↑2→p3;
 1→p4;0→p5;1→p6
60: p5+1→p5;-
 p4p3/p5↑2→p7
61: if abs(p7-
 p4)>1e-6;p6+
 p7→p6;p7→p4;
 sto -1
62: if p2=2;sto
 +12
63: ret p6
64: 8p1→p3;1→p4;
 1→p5;0→p6→p7
65: p6+p4→p6
66: p5+2→p5
67: -2p4p5↑2/
 (p5+1)p3→p8;p7+
 p8→p7
68: p5+2→p5;2p6p
 5↑2/(p5+1)p3→p4
69: if abs(p4-
 p8)>1e-6;sto -4
70: rad;p1-.7853
 98→p9
71: r(.63662/
 p1)(p6cos(p9)-
 p7sin(p9))→p6
72: if p2=2;sto
 +2
73: ret p6
74: if p1>10;
 sto +7
75: if p1=0;rst
 0
76: (p1/2)↑2→p3;
 0→p5;p1/2→p1→p8
77: p5+1→p5;-
 p3p4/p5(p5+1)→p
 7
78: if abs(p7-
 p4)>1e-6;p7→p4;
 p7+p8→p8;sto -1
79: if p2=2;ret
 2p8/p1-p6
80: ret p8
81: 0→p5;1/8p1→p
 3;1→p4;1→p2;
 0→p8
82: p5+1→p5;-
 p4p3(2p5-3)(2p5
 +1)/p5→p4
```

TABLE 3 (continued):

```
83: p4+p9→p9
84: p5+1→p5;p4p3
 (2p5-3)(2p5+1)/
 p5→p7
85: if abs(p7-
 p4)>1e-6;p7→p4;
 p7+p8→p8;gto -3
86: rad;r(.63662
 /p1)(p8cos(p1-
 .75π)-p9sin(p1-
 .75π))→p8
87: if p2=2;ret
 2p8/p1-p6
98: ret p8
*24670
```

References

[1] A. W. Love, Electromagnetic Horn Antennas, Part IV, IEEE Press, 1976.

[2] M. E. J. Jenken, "Frequency-Independence and Symmetry Properties of Corrugated Conical Horn Antennas with Small Flare Angles," NTIS #N71-10474, 1971.

[3] S. K. Buckmeyer, "Corrugations Lock Horns with Poor Beamshapes," Microwaves, p. 44, January 1973.

[4] G. R. Loefer, J. M. Newton, J. M. Schuchardt, and J. W. Dees, "Computer Analysis Speeds Corrugated Horn Design," Microwaves, p. 58, May 1976.

[5] C. Dragone, "Characteristics of a Broadband Microwave Corrugated Feed: A Comparison between Theory and Experiment," The Bell System Technical Journal, p. 869, Vol. 56, 1977.

[6] C. Dragone, "Reflection, Transmission, and Mode Conversion in a Corrugated Feed," The Bell System Technical Journal, p. 835, Vol. 56, 1977.

[7] P. D. Potter, "A New Horn Antenna with Suppressed Sidelobes and Equal Beamwidths," Microwave Journal, p. 71, June 1963.

[8] R. Caldecott, C. A. Mentzer, L. Peters and J. Toth, "High Performance S-Band Horn Antennas for Radiometer Use," NASA CR-2133, 1973.

[9] A. J. Terzuoli, Jr., and L. Peters, Jr., "VSWR Properties of E-Plane Dihedral Corrugated Horns," IEEE Trans. Ant. and Prop., AP-26, 239, 1978.

[10] A. J. Terzuoli, Jr., J. H. Richmond and L. Peters, Jr., "The VSWR of E-Plane Dihedral Horns," IEEE Trans. Ant. and Prop., AP-26, 236, 1978.

[11] B. MacA. Thomas, "Design of Corrugated Conical Horns," IEEE Trans. Ant. and Prop., AP-26, 367, 1978.